Fuel 232 (2018) 591–599

Contents lists available at ScienceDirect

Fuel

journal homepage: www.elsevier.com/locate/fuel

Full Length Article

Anchoring mechanisms of methane/air premixed flame in a mesoscale diverging combustor with cylindrical flame holder

Jianlong Wan, Cheng Shang, Haibo Zhao*

State Key Laboratory of Coal Combustion, School of Energy and Power Engineering, Huazhong University of Science and Technology, Wuhan 430074, China

ARTICLE INFO

Keywords:
Cylindrical flame holder
Diverging combustor
Flame structure
Conjugate heat exchange
Preferential transport

ABSTRACT

A mesoscale diverging combustor with a cylindrical flame holder is developed to improve the flame stabilization in present work for the first time. The experimental results show that the flame in the combustor with holder can remain symmetrically stable within a quite wide range of equivalence ratio. Then, the flame-anchoring mechanisms are analyzed systematically in terms of flow structure, conjugate heat exchange and preferential transport effect via numerical simulation. As the flame root and top attach to the flame holder and combustor, it can be deduced that the flow boundary layer very near the wall has the anchoring effect on the flame, so does the conjugate heat exchange. On the one hand, the upstream flame holder and combustor wall can preheat the incoming unburned mixture via conducting heat from the downstream solid walls, which provides a beneficial ignition condition. On the other hand, there are flame-wall coupling effects between the flame root/top and flame holder/combustor wall providing the suitable locations for flame anchoring. The anchoring locations of flame root and top show the almost same sensibility responding to the thermal conductivity of solid material. However, the anchoring temperature of flame top is more sensitive than that of flame root. In addition, the local equivalence ratios at the locations of the flame root and top are lower than the corresponding incoming equivalence ratio, which means that a better heat recirculation effect is not good for the flame-anchoring if only considering the preferential transport effect. In summary, the addition of flame holder can remarkably improve the flame stabilization and suppress the unstable flame in the combustor. This is beneficial for the application of the combustor with the diverging structure.

1. Introduction

As is known, it is very hard to maintain a stable flame in micro-/meso-scale combustors mainly due to the large surface-area-to-volume ratio and the short residence time of gaseous mixture [1,2]. Owing to those issues, many unstable flame behaviors were observed in micro-/meso-scale combustors [3,4]. For instance, Maruta et al. [3] experimentally studied the flame propagation characteristics of methane/air premixed mixture in a narrow tube with a temperature gradient. They observed the pulsating flame and the flame with repetition of extinction and ignition under a moderate flow rate. Xu and Ju [5] observed four propagation modes in a mesoscale diverging tubular combustor experimentally: the propagating flame, self-extinguished flame, stabilized planar flame and spinning flame. In addition, the spinning flame with high frequency was also found by Deshpande and Kumar [6] in a mesoscale tube combustors with two/three steps, and they pointed out that the characteristics of spinning flame were significantly influenced by the flow rate and equivalence ratio. Akram and Kumar [7] studied the flame propagation modes of methane/air premixed mixture in a meso-scale diverging combustor, and they found the flames of planar, negatively stretched and positively stretched. Obviously, these unstable flame propagation modes impede the extensive application of the combustors with the diverging structure.

Many researchers developed various special structures to improve the flame stability based on the effects of heat recirculation, flow recirculation, porous media and so on. For example, Kim et al. [8] and Kuo et al. [9] used the “Swiss-roll” configuration which could excellently preheat the unburned fuel mixture to stabilize lean flames in small combustors, and their results demonstrated that the flammability limits of fuel mixture could be significantly extended. Federici and Vlachos [10] studied the flame stability in a small combustor of single-pass heat recirculation and pointed out that the heat recirculation effect could significantly affect the blow-out limit. Veeraragavan [11] pointed out that the wall made of orthotropic thermal conductivity material could create “hot pockets” in it to stabilize the flame propagation in a plate burner. The inert porous media also can obviously expand the

* Corresponding author at: State Key Laboratory of Coal Combustion, Huazhong University of Science and Technology, 1037 Luoyu Road, Wuhan 430074, China.
E-mail address: hzhao@hust.edu.cn (H. Zhao).

https://doi.org/10.1016/j.fuel.2018.06.027
Received 23 March 2018; Received in revised form 19 May 2018; Accepted 7 June 2018

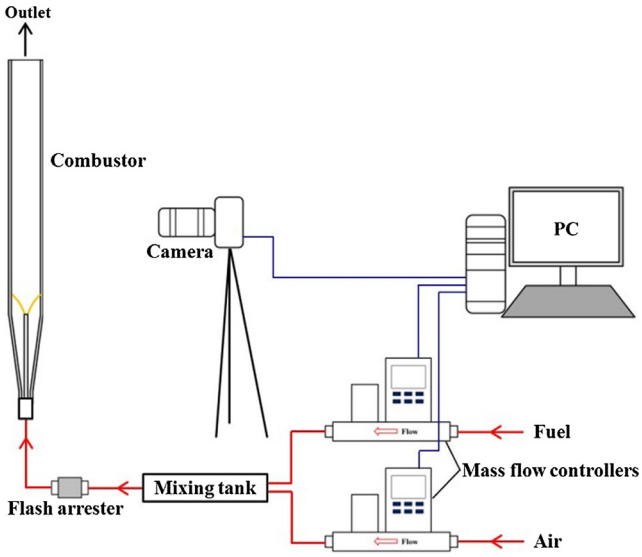

Fig. 1. Schematic view of the experimental system.

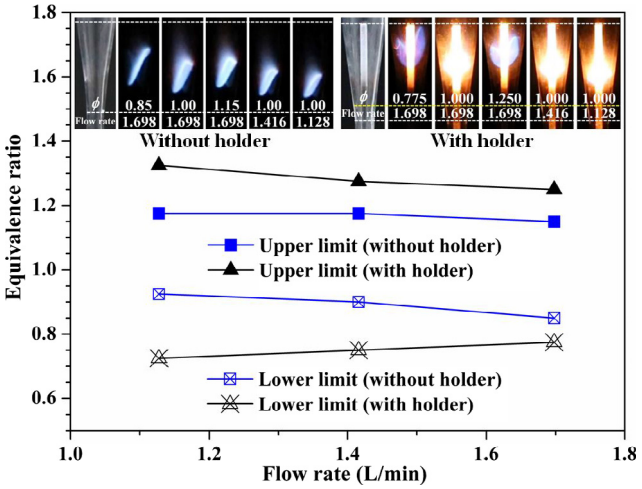

Fig. 3. Stable flame patterns at different flow rates in the mesoscale diverging combustor with/without cylindrical flame holder.

operating ranges of flow rate and equivalence ratio [12–14]. In addition, it was found that the operational limits of inlet velocity in micro combustors with one backward facing step which could generate the flow recirculation were enlarged [15,16]. Khandelwal et al. [17] experimentally demonstrated that the flame stability limits in the micro-combustor with three rearward steps were expanded significantly. Wan et al. [18–20] developed the mesoscale combustors with wall cavities and bluff-body which made excellent flame stability.

However, the above flame-anchoring strategies were mostly used in the combustor with a constant channel width. Most practical combustors have variable chamber width [5], and the attentions on improving the flame stabilization are not enough. Particularly, there is not any literature reporting the flame-anchoring methods for the diverging combustor. Recently, we noted that the wire insertion which can enhance the flame-wall coupling effect had a significant effect on improving the flame stabilization in a micro combustor with backward facing step [21]. Besides, Yang et al. [22] found that the block insertion could not only obviously increase the average combustor-wall temperature but also improve the flame stability in similar combustor. Therefore, it can be seen that the enhanced flame-wall coupling effect can obviously improve the flame stabilization.

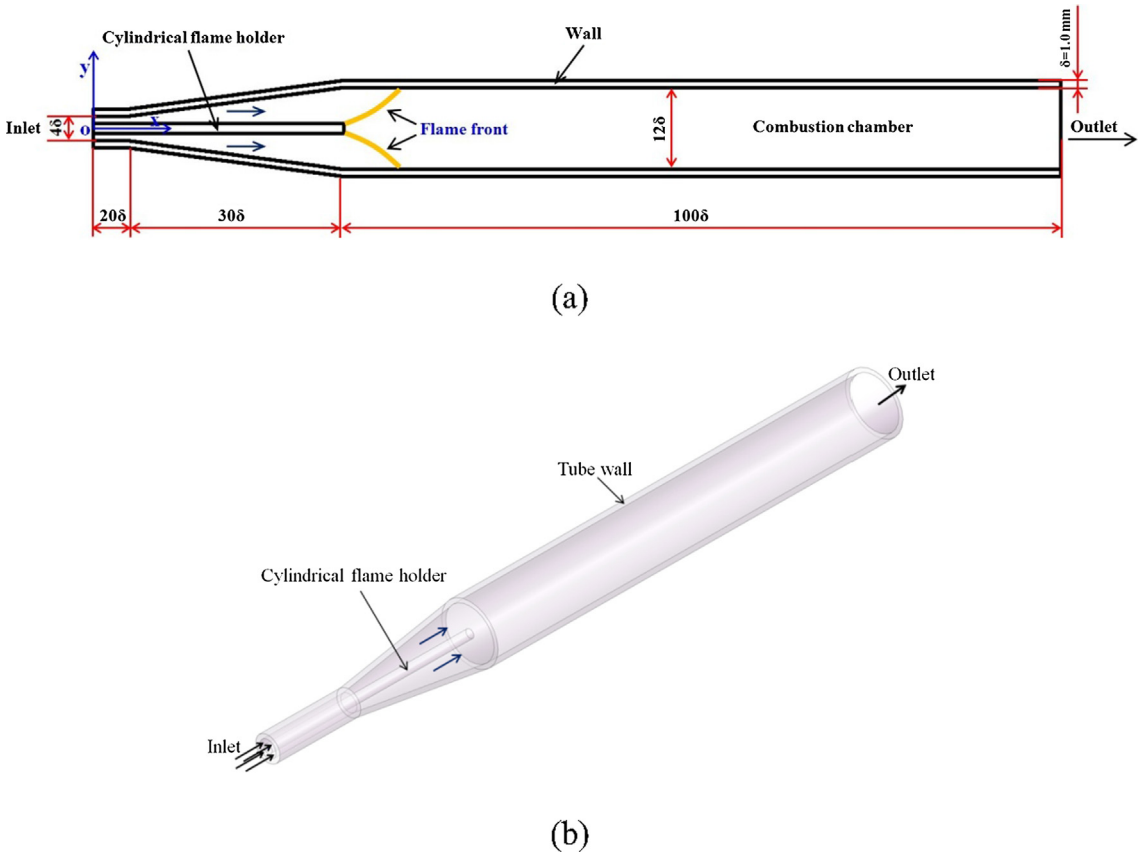

Fig. 2. Cross-section (a) and three-dimensional (b) schematics of the mesoscale diverging combustor with cylindrical flame holder.

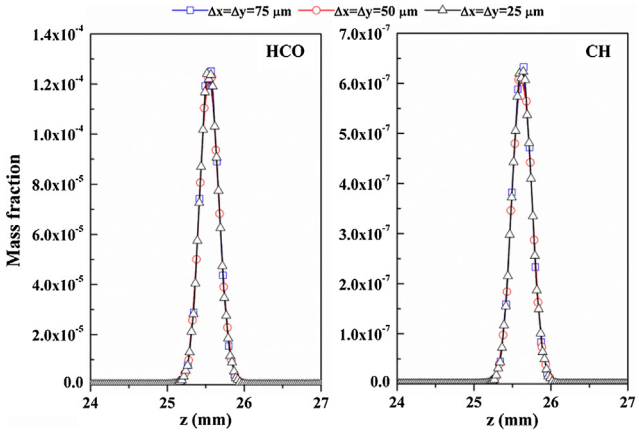

Fig. 4. Local profiles of mass fractions of HCO and CH near the flame front (y = 3.0 mm, 24.0 mm ≤ x ≤ 27.0 mm) in the diverging combustor with flame holder for three different grid resolutions at ϕ = 1.00 and Q_{in} = 1.698 L/min (V_{in} = 3.0 m/s).

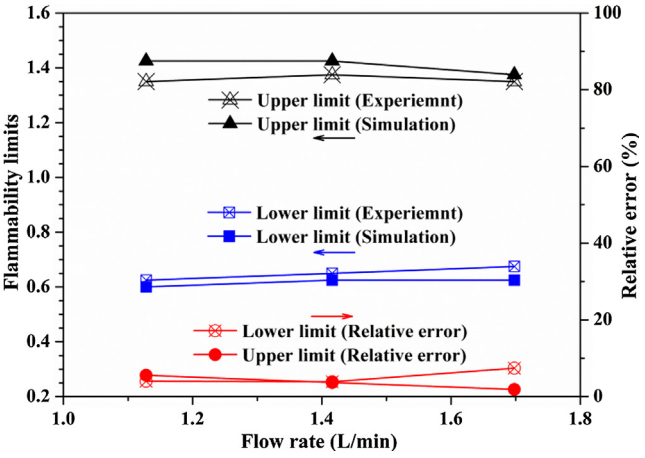

Fig. 5. Flammability limits via experiment and numerical simulation for different inlet velocity.

In this paper, a cylindrical flame holder which increases the flame-wall coupling effect is employed in the mesoscale diverging combustor to improve flame stability. It is expected to obtain the symmetrically stable flame in the wide operating condition. This combustor can be used as heat source and impetus for the mesoscale TPV (Thermophotovoltaic) system and propelling devices, respectively. We experimentally observe flame behaviors in a mesoscale diverging combustor with/without a cylindrical flame holder at first. The equivalence ratio ranges of stable flames under different flow rates are also compared. Then, the anchoring mechanisms stabilized by the flame holder are carefully analyzed in terms of flow structure, conjugate heat exchange and preferential transport effect via numerical simulation. The present work can give hints to improve the flame stabilization in the practical combustors with variable channel-width.

2. Experimental

2.1. Experimental system and methods

Fig. 1 schematically presents the experimental system. Methane and air are fully mixed in a mixing tank before entering the combustor via stainless steel pipe of 1/4 in. A digital video camera (Canon EOS 6D with the recording frequency of 25 Hz) is used to take photographs with a shutter speed of 1/180 s and capture flame behaviors. A flame gun is applied to ignite the fuel mixture at the exit of the combustor. We manufacture two mesoscale diverging combustors using the transparent quartz glass with a thermal conductivity of 2.0 W/(m·K), one with a cylindrical flame holder and another without. The geometry of two diverging combustors is same. Here we just present the geometrical structure of the combustor with the holder in Fig. 2.

Fig. 2a shows that the wall thickness (δ) is 1.0 mm. The diameter of the cylindrical flame holder is 2.0 mm, and the gap distance between the flame holder and inner wall at the inlet of combustor is 1.0 mm. The total height of the combustor is 150.0 mm. For the sake of a clear description, the whole combustor channel is divided into three segments, namely, the inlet section (20δ), the diverging section (30δ) and the straight section (100δ). In addition, Fig. 2b shows the three-dimensional geometry of this combustor, which indicates that the combustor is an axial symmetry structure.

At the beginning of the experiment, the fresh fuel mixture is ignited at ϕ = 1.0, allowing the flame to stabilize in the diverging section. Then, under a constant inlet velocity, the equivalence ratio is decreased with a step of 0.025 until flame blow-off occurs. Three flow rates (Q_{in}) are adopted, which are 1.128 L/min, 1.416 L/min and 1.698 L/min, respectively. The corresponding V_{in} in the diverging combustor without the cylindrical flame holder are 1.50 m/s, 1.875 m/s and 2.25 m/s, respectively. With respect to another one, the corresponding V_{in} are 2.0 m/s, 2.5 m/s and 3.0 m/s, respectively.

2.2. Experimental results

Fig. 3 shows the stable flame patterns at different flow rates in the mesoscale diverging combustor with/without the cylindrical flame holder. It can be seen that the stable flame are all inclining in a narrow range of equivalence ratio in the combustor without the flame holder. However, with the existence of flame holder, the flame can remain axisymmetrically stable in a wide range of the equivalence ratio around the stoichiometric ratio. In addition, our experimental result demonstrates that the flame holder can disappear the x-shape oscillating flame which occurs in the combustor without the holder. These results indicate that the flame holder can obviously suppress the dynamic flame and improve the flame stability, and its effect mechanisms will be discussed quantitatively in the following sections. Therefore, the following numerical simulation is carried out just for the diverging combustor with the flame holder.

3. Numerical simulation

3.1. Computation scheme

The computational fluid dynamics software Fluent 14.0 is applied to solve the momentum, mass, energy and species conservation equations [23]. The detailed C1 chemistry mechanism is adopted to simulate CH_4/air premixed combustion [24]. The thermodynamic and transport properties of the gaseous species are taken from the CHEMKIN databases [25]. The present work adopts the multi-component model, and does not considerate the Soret effect (Law pointed out that the Soret (second-order) diffusion is generally much smaller than the Fickian (first order) diffusion [26]). Since the heat conduction from the high-temperature combustion products to premixed reactants via solid wall can observably affect the combustion process and flame propagation characteristics [11], the heat transfer is taken into consideration in the computation. The method of “two-sided walls” is used to calculate the internal heat transfer between the gaseous mixture/flame and solid [23]. For the wall zone having a fluid and a solid region on each side (called the “two-sided wall”), a “shadow” zone is created so that each side of the wall is a distinct wall zone, and the method of “Coupled” is adopted to calculate heat transfer directly from the profiles in the adjacent cells. The heat fluxes in the fluid and solid wall are computed using the Fourier's law. In order to study the influence of the intensity of flame-wall coupling on flame stabilization, quartz (the same as the

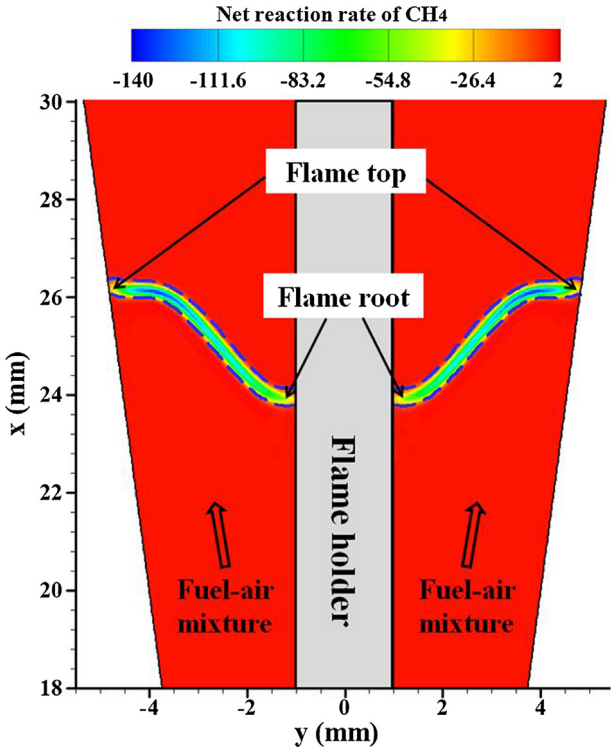

Fig. 6. Net reaction rate contours of CH_4 with overlaid normalized isolines of 10% of maximum Y_{HCO} mass fraction (blue dashed line) at $\phi = 1.00$ and $Q_{in} = 1.698$ L/min ($V_{in} = 3.0$ m/s). (For interpretation of the references to colour in this figure legend, the reader is referred to the web version of this article.)

experimental combustor material), steel and silicon carbide (SiC) are selected as solid materials in the computation, whose thermal conductivities are 2.00 W/(m·k), 12.0 W/(m·k) and 32.8 W/(m·k), respectively [27]. The heat loss from the exterior wall of the preheating channels includes natural convection and radiation, and they are calculated according to Ref. [28].

The inner wall surfaces are assumed to be chemically inert with a no-slip boundary condition. The CH_4/air mixture of 300 K with uniform concentration and velocity distributions is set at the inlet of combustor. A Neumann boundary condition is given for the exit. Grid independency is checked using three sets of grid system ($\Delta x = \Delta y = 75$ μm, 50 μm and 25 μm, respectively). When comparing the profiles of two key radicals (HCO and CH) near the flame front, the cell size of 75 μm is sufficiently fine to capture the flame structure. Further refinement is conducted on the meshes near the cylindrical flame holder (Fig. 4).

3.2. Model validation

To evaluate the accuracy of the present numerical model, we compare the experimental measurements and numerical results of the flammability limits based on equivalence ratio, as shown in Fig. 5. The predicted flammability limit was obtained via steady-state simulation. It is noted that the predicted and measured flammability limits are approximately equal. The maximum relative error is 7.41% for the lower limit, while the minimum is only 1.85% for the upper limit. These results indicate that the numerical model/method adopted in this work is reasonable.

3.3. Results and discussion

3.3.1. Definition of flame front

It is confirmed that the radical HCO strongly correlates with the heat-release rate in the combustion processes of hydrocarbon fuels [29]. The article of Kedia and Ghoniem [30] as well as our previous work [28,31] showed that the mass fraction of HCO (Y_{HCO}) could be used to mark the flame front appropriately. Here, we use the same definition for the flame front. We present the net reaction rate contours of CH_4 with overlaid normalized isolines of 10% of the maximum Y_{HCO}, which has been normalized by their maximum values, in Fig. 6. It is evident that the high reaction rate zone of CH_4 lies in the scope of normalized isolines of 10% of maximum Y_{HCO}. Similar structures are also observed in other cases. Therefore, we use the normalized 10% of maximum Y_{HCO} isoline to visualize the flame front.

3.3.2. Flame structure

At first, Fig. 7 presents the flow structure, which indicates that there

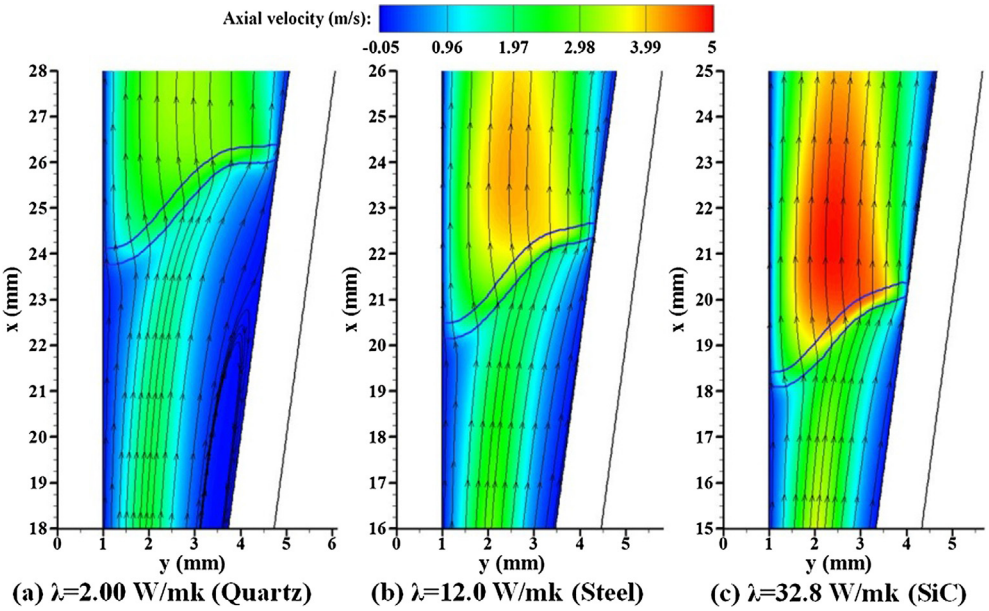

Fig. 7. The axial-velocity contours with overlaid 10% maximum Y_{HCO} isolines and flow streamline near the flame front for different solid materials at $\phi = 1.00$ and $V_{in} = 3.0$ m/s.

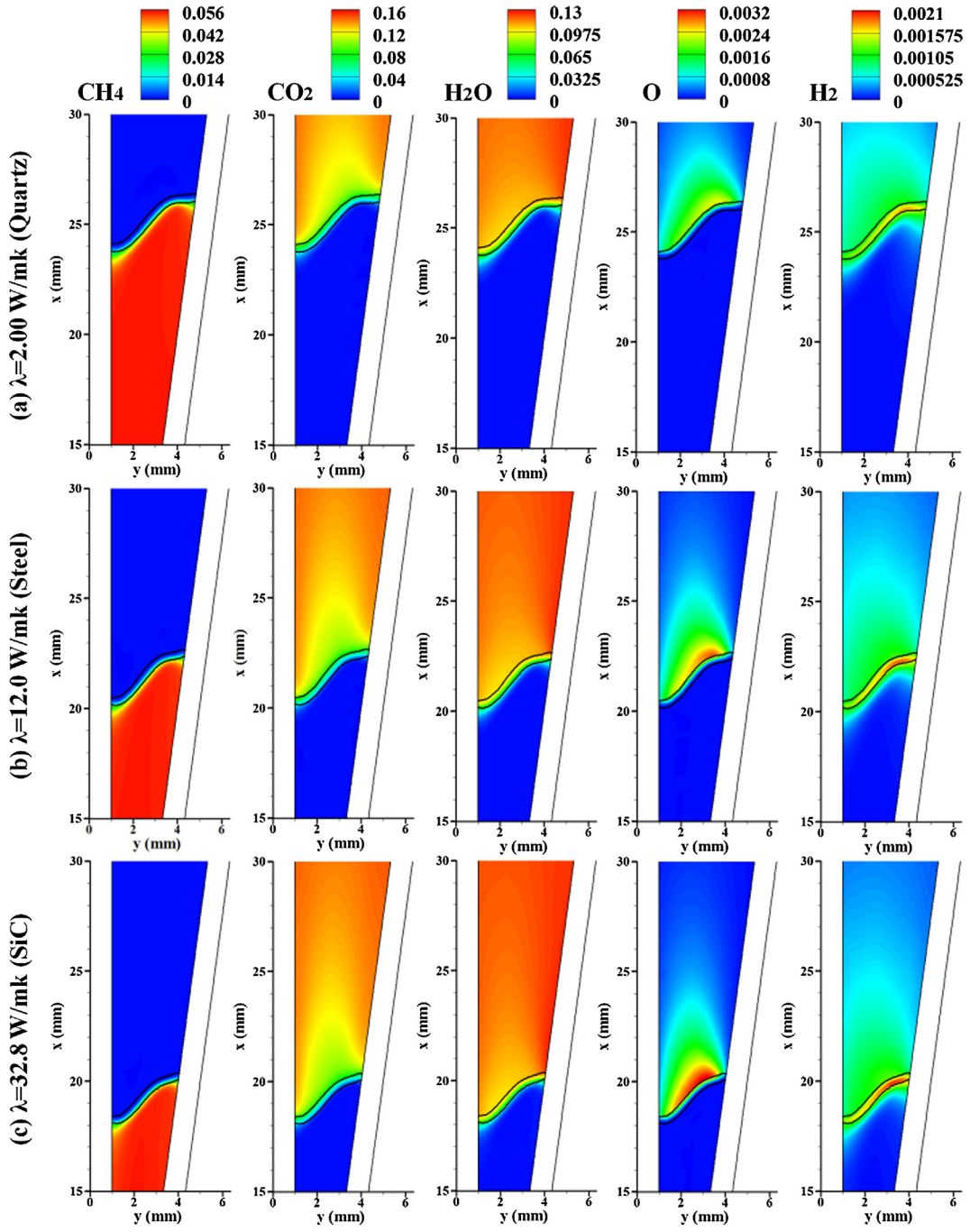

Fig. 8. Main species contours with overlaid 10% maximum HCO isoline (black lines) near the flame front for different solid materials at $\phi = 1.00$ and $V_{in} = 3.0$ m/s.

are no recirculation zones near the flame root and top. The flame root and top attach to the vertical wall of flame holder and inner wall of diverging section, respectively. It can be deduced that the flow boundary layer very near the wall has the anchoring effect on the flame front. In addition, the larger flow velocity and temperature gradients around the flame front combining with the obvious flow two-dimensionality can significantly affect the flame structure (as shown in Fig. 8).

Fig. 8 shows the main species contours with overlaid 10% maximum Y_{HCO} isoline near the flame front. This figure indicates that the flame structures for three solid materials are almost same even though their anchoring locations of flame front are different. It can be seen that the CH_4 (reactant) concentration gradient near the flame front decreases when approaching the walls (vertical wall of flame holder or inner wall of diverging section), and it is completely consumed just behind the preheat zone of flame front. There is a little difference in the distribution characteristics of combustion products (CO_2 and H_2O). The high concentration zones of CO_2 and H_2O mainly appear near the walls. However, the H_2O exists just in front of the flame front in the preheating zone. This difference is mainly caused by the different diffusion velocities of CO_2 and H_2O. The maximum diffusion velocity of H_2O is almost twice faster than that of CO_2 [32,33]. As a result, H_2O can diffuse more upstream. In addition, some intermediate species of small molecular weight (such as O and H_2) diffuse and convect towards the preheating zone, which is more remarkable for H_2 owing to its faster diffusion velocity. The O radical nearly disappears near the wall with the relative low-temperature wall caused by the recombine effect. The stronger chemical reaction in the combustor with a larger thermal

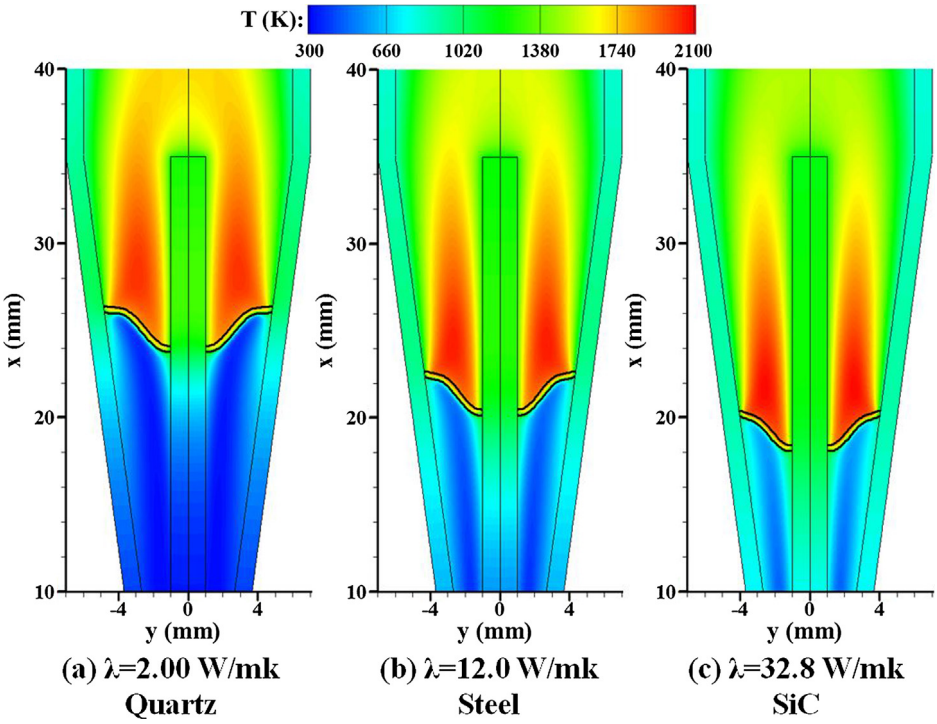

Fig. 9. The temperature contours with overlaid 10% maximum Y_{HCO} isoline (black lines) near the flame front for different solid materials at $\phi = 1.0$ and $V_{in} = 3.0$ m/s.

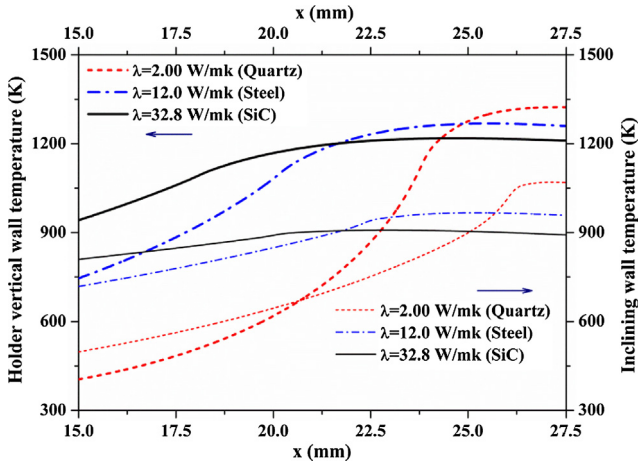

Fig. 10. Vertical wall temperature profiles of flame holder ($y = 1.0$ mm, 15.0 mm $\le x \le$ 27.5 mm) and inner wall temperature profiles of diverging section (2.67 mm $\le y \le$ 4.92 mm, 15.0 mm $\le x \le$ 27.5 mm) near the flame front for different solid materials at $\phi = 1.0$ and $V_{in} = 3.0$ m/s.

conductivity results in a higher concentrations of O and H_2.

3.3.3. Conjugate heat exchange

It is recognized that the conjugate heat exchange between gaseous mixture and solid wall has a significant effect on flame stabilization [11,34]. The heat is transferred from the hot burned mixture to the combustor wall and cylindrical flame holder, and then preheats the incoming unburned mixture. Subsequently, this preheating effect will affect the flame propagation characteristics. Fig. 9 demonstrates that a larger thermal conductivity of solid material results in a better preheating effect (also shown in Figs. 10 and 11). As a result, the combustion reactions occur in a more upstream location, and the faster burning velocity can reach a static balance with the faster flow velocity in a narrower flow channel. Therefore, the flame front shifts upstream and becomes lower as the increase in the thermal conductivity.

It can be calculated from Fig. 10 that the average vertical wall temperatures of the flame holder made of quartz, steel and SiC are 824.3 K, 1095.7 K and 1148.5 K, respectively. However, the maximum temperatures of them are 1323.6, 1268.1 and 1218.2 K. In addition, the average inner-wall temperatures of diverging section near the flame front are 732.6 K, 874.7 K and 881.1 K for quartz, steel and SiC materials, respectively. Whereas, the maximums of inner-wall temperature for them are 1070.1 K, 966.8 K and 908.4 K. In other words, as the increase of thermal conductivity, the average wall temperature near the flame front is increasing because the solid wall with a larger thermal conductivity can transport more heat from the downstream wall to the upstream wall, but the maximum of wall temperature is decreasing. This is because that a larger thermal conductivity results in a higher heat flux into the solid wall, which leads to a larger temperature difference between the wall and burned mixture. As the temperatures of burned mixture near the combustor walls are almost same (see Fig. 9), the maximum of wall temperature is smaller for the solid material with a larger thermal conductivity. However, the inner wall with higher average temperature preheats better, as presented in Fig. 11.

Fig. 11 indicates that the gas temperatures level is higher for a larger thermal conductivity. The average temperature of fresh mixture at $x = 16.25$ mm is 392.9 K, 572.6 K and 698.7 K for quartz, steel and SiC, respectively. As a result, a larger thermal conductivity results in earlier initiation of chain reactions and more intense combustion reaction, which can significantly affects the anchoring locations and anchoring temperatures of flame root and top.

As shown in Fig. 12, when the thermal conductivity or equivalence ratio is decreasing, the flame root and top obviously shifts downstream, which means that the anchoring locations significantly depend on the thermal conductivity of solid material. In addition, the displacement amplitudes of flame top and flame root are almost same, which indicates that they have almost same sensitive for the thermal conductivity.

The conjugate heat exchange also significantly affects the anchoring temperatures of flame root and top. Fig. 13 indicates that the anchoring

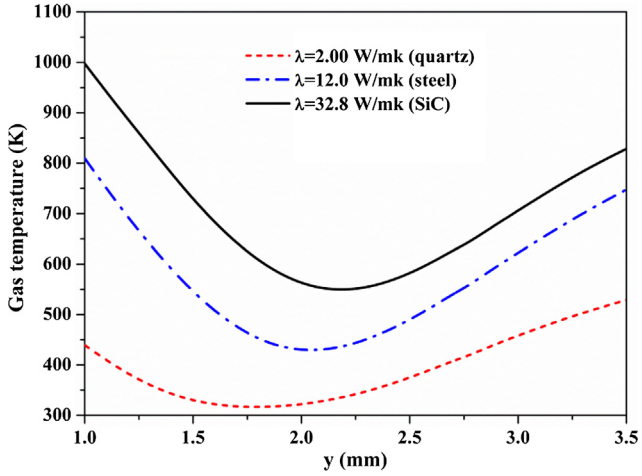

Fig. 11. Unburned mixture temperature profiles at x = 16.25 mm in front of the flame front for different solid materials at ϕ = 1.0 and V_{in} = 3.0 m/s.

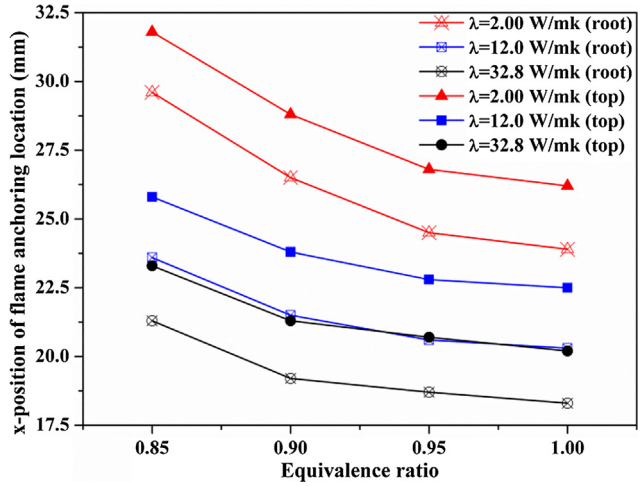

Fig. 12. The x-positions of anchoring locations of flame root and flame top for different equivalence ratios and solid materials.

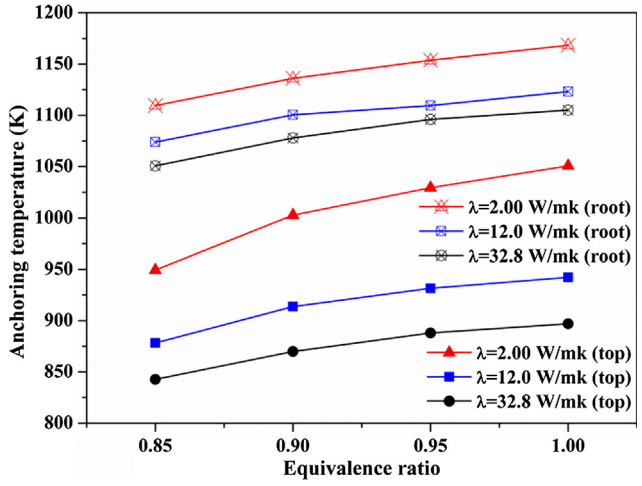

Fig. 13. The anchoring temperatures of flame root and flame top for different equivalence ratios and solid materials.

temperature decreases with the decrease in the equivalence ratio or the increase in the thermal conductivity. In addition, the anchoring temperature of flame top is obviously lower than that of flame root, which results from the significant heat loss effect of combustor wall on the flame top. The anchoring temperature difference of flame top among three materials is obviously larger than that of flame root. For example, the anchoring temperature difference between quartz and SiC is ~63.3 K, but that of flame top is ~153.8 K at ϕ = 1.0. This means that the anchoring temperature of flame top more remarkably depends on the thermal conductivity of solid material. This is probably because that the thermal conductivity can significantly affect the heat-loss rate near the flame top.

3.3.4. *Preferential transport*

The difference in mass diffusivities of different reaction species and the flow two-dimensionality can result in preferential transport effect [30,33]. The local equivalence ratio (ϕ_{local}) based on local fuel/oxygen atom balance of major species which was developed by Barlow et al. [33] is used to quantitatively evaluate this effect, as given by Eq. (1):

$$\phi_{local} = \frac{0.5(X_{H_2} + X_{H_2O}) + X_{Co_2} + X_{Co} + 2X_{CH_4}}{0.5(X_{Co} + X_{H_2O}) + X_{O_2} + X_{Co_2}} \quad (1)$$

where X is the mole fraction of species.

To observe the transverse characteristics of the preferential transport effect, Fig. 14 presents the local equivalence ratio, axial velocity and Y_{HCO} profiles for various y slices in the quartz combustor. ϕ_{local} increases firstly and then decreases in front of the flame front (see Fig. 14a and c), which is different from the result for a CH_4/air premixed flame in the combustor with a constant channel width by Kedia et al. [30] and Barlow et al. [33] (the increasing stage of ϕ_{local} does not occur). On the one hand, the flow area is smaller in a more upstream channel (*i.e.*, the concentration zone of species radicals is smaller), which induces the high concentration zones of the species with a faster diffusion velocity (such as H_2 and CO). On the other hand, Fig. 7 shows that the flow velocity near the flame top is faster, which means that more methane concentrates near the flame top (see Fig. 8). As a result, the chemical reaction rate and heat release rate are larger for a bigger y value. Subsequently, the ϕ_{local} decreases sharply and then increases just in front of the flame front (preheat zone). This is because that the diverging structure can enhance the flow two-dimensionality and the velocity gradient near the flame front is greater (see Fig. 14b), which results in the increase of local-equivalence-ratio [35]. However, there are also obvious high concentration zones of ϕ_{local} near the walls behind the flame front (high temperature products), which are also observed in other cases. This phenomenon is mainly caused by the combustion reactions of a locally richer mixture and the locally higher strain and curvature rates.

In addition, as shown in Fig. 14d, the ϕ_{local} is lower than the incoming ϕ near the flame root and top, and this phenomenon is also observed in steel and SiC combustors. Fig. 15 presents that ϕ_{local} at the anchoring locations of flame top is larger than that of the flame root, but they are both lower than the incoming equivalence ratio. Furthermore, ϕ_{local} at the anchoring location is increasing with the decrease of thermal conductivity. Combining the results in Fig. 11, it can be deduced that a better preheating effect for a larger thermal conductivity is not good for the flame stabilization if only looking at the preferential transport effect.

4. Conclusions

The anchoring mechanism of methane/air premixed flame in the diverging combustor with a cylindrical flame holder is studied in terms of flow field, conjugate heat exchange and preferential transport via numerical simulation. At first, the flame structure is investigated. The methane is completely consumed just behind the upstream boundary of flame front. The H_2O exists just in front of the flame front in the preheating zone, and it diffuses more upstream than CO_2 due to the faster diffusion velocity. The recombine effect makes the O radical nearly

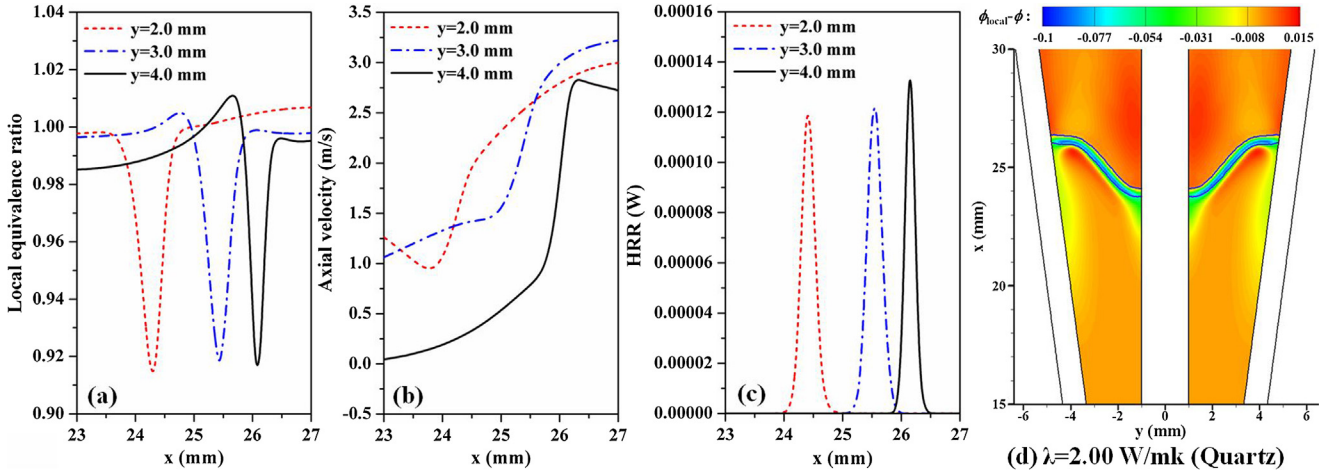

Fig. 14. Local equivalence ratio (a), axial velocity (b) and Y_{HCO} (c) profiles near the flame front for different y slices, and the colored contours of $\phi_{\text{local}} - \phi$ (departure from the incoming mixture equivalence ratio) with overlaid 10% maximum HRR isoline (d) in the quartz combustor at $\phi = 1.0$ and $V_{\text{in}} = 3.0$ m/s.

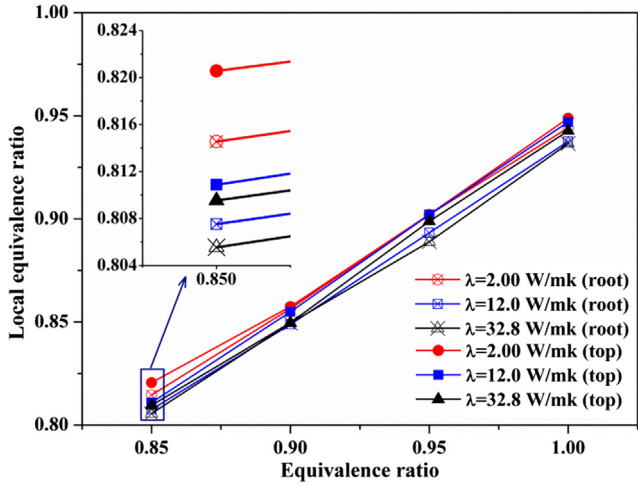

Fig. 15. Local equivalence ratios at anchoring positions of flame root and flame top for different equivalence ratio in the combustors made of three solid materials.

disappear near the solid wall with relative low temperature. As the flame root and top attach to the wall, it is deduced that the flow boundary layer very near the wall can well anchor the flame front. In addition, the low velocity zone near the wall provides a suitable region where velocity balance can be obtained for flame-anchoring. The conjugate heat exchange between the gaseous mixture and solid wall can affect the preheating effect on the incoming unburned mixture, and a larger thermal conductivity results in a higher preheating temperature, which makes the flame shift upstream. The anchoring locations of flame root and top show the almost same sensitivity for the thermal conductivity of solid material, *i.e.*, the moving amplitude of flame root and top are almost same as the decrease in the equivalence ratio. The flame anchoring temperature also critically depends on the thermal conductivity, and it is more obvious for the flame top. In particular, a larger thermal conductivity leads to a lower anchoring temperature of flame root and top. Besides, the preferential transport effect gives rise to the high local equivalence ratio zone, which presents the different distribution characteristics in the combustor with constant channel width. The ϕ_{local} at the anchoring locations of flame root is slightly lower than that of flame top, but both of them are lower than the corresponding incoming equivalence ratio. The ϕ_{local} at the anchoring locations of flame root and top show the almost same sensitivity for the thermal conductivity.

The above results indicate that there is a little difference of the anchoring mechanism in the diverging combustor comparing with the combustor owning a constant channel width. In the diverging combustor with a flame holder, the flame is mainly anchored by the flow boundary layer, low velocity zone near the wall and flame-wall coupling effect. The preferential transport effect is not the dominating factor for anchoring flame here.

Acknowledgement

This work was supported by the Natural Science Foundation of China (Nos. 51706080, 51522603) and the China Postdoctoral Science Foundation (2016M600591, 2018T110761).

References

[1] Ju Y, Maruta K. Microscale combustion: technology development and fundamental research. Prog Energy Combust Sci 2011;37(6):669–715.
[2] Chou SK, Yang WM, Chua KJ, Li J, Zhang KL. Development of micro power generators – a review. Appl Energy 2011;88(1):1–16.
[3] Maruta K, Kataoka T, Kim NI, Minaev S, Fursenko R. Characteristics of combustion in a narrow channel with a temperature gradient. Proc Combust Inst 2005;30(2):2429–36.
[4] Alipoor A, Mazaheri K. Combustion characteristics and flame bifurcation in repetitive extinction-ignition dynamics for premixed hydrogen-air combustion in a heated micro channel. Energy 2016;109:650–63.
[5] Xu B, Ju Y. Experimental study of spinning combustion in a mesoscale divergent channel. Proc Combust Inst 2007;31(2):3285–92.
[6] Deshpande AA, Kumar S. On the formation of spinning flames and combustion completeness for premixed fuel–air mixtures in stepped tube microcombustors. Appl Therm Eng 2013;51(1–2):91–101.
[7] Akram M, Kumar S. Experimental studies on dynamics of methane–air premixed flame in meso-scale diverging channels. Combust Flame 2011;158(5):915–24.
[8] Kim N, Kato S, Kataoka T, Yokomori T, Maruyama S, Fujimori T, et al. Flame stabilization and emission of small Swiss-roll combustors as heaters. Combust Flame 2005;141(3):229–40.
[9] Kuo CH, Ronney PD. Numerical modeling of non-adiabatic heat-recirculating combustors. Proc Combust Inst 2007;31(2):3277–84.
[10] Federici JA, Vlachos DG. A computational fluid dynamics study of propane/air microflame stability in a heat recirculation reactor. Combust Flame 2008;153(1–2):258–69.
[11] Veeraragavan A. On flame propagation in narrow channels with enhanced wall thermal conduction. Energy 2015;93:631–40.
[12] Hashemi SM, Hashemi SA. Flame stability analysis of the premixed methane-air combustion in a two-layer porous media burner by numerical simulation. Fuel 2017;202:56–65.
[13] Li J, Chou SK, Li ZW, Yang WM. Experimental investigation of porous media combustion in a planar micro-combustor. Fuel 2010;89(3):708–15.
[14] Li J, Wang Y, Shi J, Liu X. Dynamic behaviors of premixed hydrogen–air flames in a planar micro-combustor filled with porous medium. Fuel 2015;145:70–8.
[15] Yang WM, Chou SK, Shu C, Li ZW, Xue H. Combustion in micro-cylindrical combustors with and without a backward facing step. Appl Therm Eng 2002;22:1777–87.
[16] Yilmaz I, Yilmaz H, Cam O, Ilbas M. Combustion characteristics of premixed

hydrogen/air flames in a geometrically modified micro combustor. Fuel 2018;217:536–43.
[17] Khandelwal B, Deshpande AA, Kumar S. Experimental studies on flame stabilization in a three step rearward facing configuration based micro channel combustor. Appl Therm Eng 2013;58(1–2):363–8.
[18] Wan JL, Fan AW, Liu Y, Yao H, Liu W, Gou XL, et al. Experimental investigation and numerical analysis on flame stabilization of CH4/air mixture in a mesoscale channel with wall cavities. Combust Flame 2015;162(4):1035–45.
[19] Wan JL, Fan AW, Yao H, Liu W. Experimental investigation and numerical analysis on the blow-off limits of premixed CH4/air flames in a mesoscale bluff-body combustor. Energy 2016;113:193–203.
[20] Wan JL, Fan AW, Yao H, Liu W. A non-monotonic variation of blow-off limit of premixed CH4/air flames in mesoscale cavity-combustors with different thermal conductivities. Fuel 2015;159:1–6.
[21] Baigmohammadi M, Sarrafan Sadeghi S, Tabejamaat S, Zarvandi J. Numerical study of the effects of wire insertion on CH4(methane)/AIR pre-mixed flame in a micro combustor. Energy 2013;54:271–84.
[22] Yang WM, Jiang DY, Chua KYK, Zhao D, Pan JF. Combustion process and entropy generation in a novel microcombustor with a block insert. Chem Eng J 2015;274:231–7.
[23] Fluent 14.0. User's Guide, Canonsburg, PA; 2011.
[24] Kee RJ, Grcar JF, Smooke MD, Miller JA. Sandia National Laboratories Report, SAND85-8240; 1994.
[25] Kee RJ, Grear JF, Smooke MD, Miller JA. Sandia National Laboratories Report, SAND85-8240; 1985.
[26] Law CK. Combustion physics. Cambridge: Cambridge University Press; 2006.
[27] Ma Q, Fang R, Xiang L. Handbook of thermo-physical properties. Beijing: China Agricultural Machinery Press (in chinese); 1986.
[28] Wan JL, Fan AW, Yao H. Effect of the length of a plate flame holder on flame blowout limit in a micro-combustor with preheating channels. Combust Flame 2016;170:53–62.
[29] Najm HN, Paul PH, Mueller CJ, Wyckoff PS. On the adequacy of certain experimental observables as measurements of flame burning rate. Combust Flame 1998;113:312–32.
[30] Kedia KS, Ghoniem AF. The anchoring mechanism of a bluff-body stabilized laminar premixed flame. Combust Flame 2014;161(9):2327–39.
[31] Wan JL, Zhao H. Dynamics of premixed CH 4/air flames in a micro combustor with a plate flame holder and preheating channels. Energy 2017;139:366–79.
[32] Michaels D, Ghoniem AF. Impact of the bluff-body material on the flame leading edge structure and flame–flow interaction of premixed CH4/air flames. Combust Flame 2016;172:62–78.
[33] Barlow RS, Dunn MJ, Sweeney MS, Hochgreb S. Effects of preferential transport in turbulent bluff-body-stabilized lean premixed CH4/air flames. Combust Flame 2012;159(8):2563–75.
[34] Miguel-Brebion M, Mejia D, Xavier P, Duchaine F, Bedat B, Selle L, et al. Joint experimental and numerical study of the influence of flame holder temperature on the stabilization of a laminar methane flame on a cylinder. Combust Flame 2016;172:153–61.
[35] Katta V, Roquemore WM. C/H atom ratio in recirculation-zone-supported premixed and nonpremixed flames. Proc Combust Inst 2013;34(1):1101–8.